Ecological Indicators 162 (2024) 112036

Contents lists available at ScienceDirect

Ecological Indicators

journal homepage: www.elsevier.com/locate/ecolind

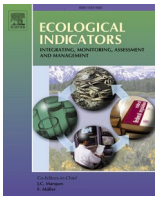

Original Articles

Large-scale wall-to-wall mapping of bark beetle damage and forest practices using the distance red swir index and operational harvester data

Henrik J. Persson [a,*], Simon Kärvemo [b], Eva Lindberg [a], Langning Huo [a]

[a] Department of Forest Resource Management, Swedish University of Agricultural Sciences (SLU), Sweden
[b] Department of Ecology, Swedish University of Agricultural Sciences (SLU), Sweden

ARTICLE INFO

Keywords:
Disturbance
Picea abies
Ips typographus
Bark beetles
Sentinel
Mapping
Harvester

ABSTRACT

Satellite-based inventories of bark beetle attacks are increasingly used for detecting and monitoring infested forest at the landscape scale. The Normalized Distance Red & SWIR index is one of few indices that have shown higher accuracies than commonly used vegetation indices. In this study, the temporal changes of the distance red swir (ΔDRS) index were analyzed, validated and applied to multi-temporal Sentinel-2 images covering one tile of 110 x 110 km^2. The main purpose was to assess the applicability of a new ΔDRS vegetation index to detect spruce forest after bark beetle (*Ips typographus*) attacks. Harvester data from a private forest company were used to validate the method. The normalized DRS index has previously been developed and tested at test site level, while this study explored and demonstrated the use of ΔDRS in an applied context on a larger scale. Water and chlorophyll induced changes and different disturbances were effectively identified across the landscape. A linear-discriminant analysis was used to classify 274 clusters as attacked and healthy forest, with an overall accuracy of 78%. The largest ΔDRS values in our study (>0.06) corresponded well to clear-cuts, and all 172 clear-cuts were correctly classified. We conclude that the ΔDRS index has a potential to map vegetation changes related to water and chlorophyll changes in the Scandinavian forests and that it can be useful to identify bark beetle-infested forest within 1 year after the attacks and clear-cuts.

1. Introduction

Bark beetle outbreaks are a significant biotic disturbance in temperate forests (Sommerfeld et al., 2018), often leading to alterations in both biotic and abiotic conditions. These changes include decreased canopy cover, greater amounts of dead wood, and variations in stand ages and tree species composition, all of which contribute to biodiversity enhancement (Beudert et al., 2015; Lehnert et al., 2013). Simultaneously, bark beetles cause large economic forest damages. During the first two years of the ongoing outbreak in Sweden, 10–11 million m^3 of timber were lost, while the Czech Republic required 260 million EUR in state interventions to address related issues (Hlásny et al., 2021; Huo et al., 2021). The occurrences of disturbances, and in particular bark beetle outbreaks, have increased drastically in the recent decades which partly can be attributed to the higher temperatures resulting from climate change, as well as increased homogeneity in managed forests which increase host availability (Raffa et al., 2015). The bark beetles benefit from higher temperatures as they exploit the weakening of host tree defenses caused by drought, and consequently, fewer beetles are needed to kill a tree under such circumstances. In addition, warmer summers shorten the generation time and thus increase the number of annual generations. The homogenous mono species plantations decrease resilience to natural disturbances in general (Jactel et al., 2017). This is obvious also for bark-beetle outbreaks where large host-tree volumes strongly increase infestation risks (Kärvemo et al., 2016; Pasztor et al., 2014). Furthermore, forest management that includes clear-cuts expose more forest to distinct borders, which is known to increase the number of bark beetle attacks due to a changing microclimate (Hedgren et al., 2003; Kautz et al., 2013) and host-tree volatiles (Hedgren et al., 2003). For some bark beetle species, such as the European spruce bark beetle *Ips typographus*, infested trees are commonly situated in small clusters or infestations patches. In Sweden, >80 % of the clusters contain fewer than 25 trees (Kärvemo et al., 2023) and in Slovakia 79 % were clustered within areas smaller than 500 m^2 (Potterf et al., 2019). Methods are needed both for wall-to-wall mapping to support forest management decisions and for monitoring of damage levels at region and country level (Hanewinkel et al., 2008; Pasztor et al., 2014; Patacca et al., 2023).

Remote sensing (RS) has increasingly been used as an efficient mean

* Corresponding author.
E-mail address: Henrik.Persson@slu.se (H.J. Persson).

https://doi.org/10.1016/j.ecolind.2024.112036
Received 12 September 2023; Received in revised form 12 April 2024; Accepted 12 April 2024
Available online 16 April 2024

to identify and map disturbances wall-to-wall over large areas (Candotti et al., 2022; Estrada et al., 2023; Luo et al., 2023; Mandl and Lang, 2023; Trubin et al., 2023). Methods that are feasible to map bark beetle attacked forest can often be efficient means to map also other damage types, e.g. wind throws (Candotti et al., 2022; Tanase et al., 2018). In the recent works aimed at addressing bark-beetle outbreak challenges, early detection and rapid management actions have been proposed as one crucial component (Abdullah et al., 2019; Gao et al., 2022; Luo et al., 2023; Ortiz et al., 2013; Tanase et al., 2018; Trubin et al., 2024; Yu et al., 2022). Effective sanitation felling of infested trees requires that the trees are cut before the adult beetles emerge (Wermelinger, 2004). In southern Sweden, 50 % of the filial beetles have been found to emerge 11 weeks after the brood was initiated (Öhrn et al., 2014). Within the vegetation period, an average time-lag of two to three months is commonly needed until the *I. typographus* infestation can be reliably detected in aerial surveys (Huo et al., 2023, 2021; Jactel et al., 2017; Kautz, 2014).

In a previous work, we developed a vegetation index based on two spectral bands from Sentinel-2 (S2), denoted normalized distance red & swir (NDRS), (Huo et al., 2021), where its spectral response due to the changing tree physiology was discussed in Section 5.1. This index was used to classify bark-beetle attacked forest in a relatively small Swedish test site (1,600 ha) and it has since been both tested and compared with other indices, and evaluated across other European forest types, e.g., in the European Alps (Candotti et al., 2022; Dalponte et al., 2022; Huo et al., 2023; Jamali et al., 2023). The normalization requires known locations of spruce stands, which may not be available. The steps toward an applied use of the NDRS index have motivated us to explore the relationship of the DRS index to bark beetle attacks, and furthermore assess the performance, in an environment relevant for boreal forestry, and in a large-scale operational setting. Most other studies have focused on test site level or used high-resolution data that are not suitable for wall-to-wall monitoring. The analyses in this paper extend previous bark beetle mapping efforts based on satellite (Bárta et al., 2021; Candotti et al., 2022; Dalponte et al., 2022; Huo et al., 2021; Jamali et al., 2023) and aerial data (Bárta et al., 2022; Kärvemo et al., 2014). Several of them focused on early detection (Bárta et al., 2021,2022, Candotti et al., 2022, Huo et al., 2021, Jamali et al., 2023), and some used sensors allowing the work to be carried out at single-tree level, e.g, high-resolution hyperspectral imagery or lidar, (Bárta et al., 2022; Dalponte et al., 2022; Huo et al., 2023). Both Candotti et al. (2022) and Dalponte et al. (2022) investigated the use of multiple S2 bands or multiple vegetation indices based on S2, applied to bark beetle attacked trees in the Alp region. Jamali et al. (2023) focused on the early detection in Sweden using S2 data. Early detection has proven to be challenging and not providing consistent results. Nevertheless, mapping of bark beetle-attacked trees in later stages is also beneficial for forest management, but has not yet been successful operationally. For example, 72 % of the trees in Sweden killed by bark beetles are still not removed, causing dangerous conditions with dead standing trees (Wulff and Roberge, 2023). Comparisons of study results are not straightforward, due to different study designs, spatial scales (of trees and sensor resolution), validation metrics, and extent of study areas. Furthermore, only studies based on balanced data samples can to some degree be compared. Yet, we think that a single method for mapping bark beetle attacked trees over large areas with high accuracy is still missing. A number of criteria should hence be met: the method should provide such accuracy that it is operationally useful, the area of interest should span considerably more forest than a single test site or local ecosystem, the method works with data available wall-to-wall to enable monitoring (i.e., an alert system could be implemented), the method is useful for the later attack stages too – early detection is not realistic for most operational forestry, the method does not require extensive complementary data (e.g, pheromon traps, recent laser scanning data or other high-resolution data unavailable at large-scale), and at best – the method works regardless of geographic region.

Several studies adressing many of these criterias have demonstrated the potential of using Landsat (Senf et al., 2015) or S2 data (Barta et al. 2021, Candotti et al. 2023, Dalponte et al. 2023, Jamali et al., 2023), with Senf et al. (2015) adressing a forest in British Columbia, the first three S2 studies adressing temperate forest in the alps, and Jamali et al., 2023 adressing the early detection of boreal forest. Yet, the demonstration of a bark beetle damage map of boreal forest with useful accuracy is yet sparse or non-existing.

The main focus of this study is the testing, applied use, and evaluation of ΔDRS (temporal DRS change) in a large-scale context suitable for national operational forest monitoring, and building upon operational reference data. The objectives were to 1) generate a large-area forest map indicating bark beetle attacks (not addressing early detection specifically), 2) assess the accuracy of the map(s) in an operational relevant environment, and 3) identify and share other useful experiences related to the mapping method(s).

2. Material and Methods

2.1. Study site and reference data

The study was conducted in Sweden (northern Europe), located mainly in the boreal forest region, though the southernmost parts are within the hemi-boreal and nemoral regions. In 2018, an extensive drought hit Europe and Sweden (Rousi et al., 2023). Consequently, many spruce trees reduced their vitality and suffered from large-scale attacks by the spruce bark beetle. Large areas of southern Sweden were particularly exposed and the largest forest company in the area (Södra) provided harvester data for their forests in both 2018 and 2019. During this period, there were unfortunately few cloud-free images and due to this, we selected a single Sentinel-2 tile (33VWD) covering 110 × 110 km^2 as study area (Fig. 1). This is located in southeastern Sweden and had the best combination of cloud-free images and harvester data available as ground reference. The forest in the area is dominated by Norway spruce (*Picea abies* (L.) H. Karst.), Scots pine (*Pinus sylvestris* L.) and birch (*Betula* spp.), where pine (30 %) and spruce (46 %) constitute most of the volume (SLU, 2019). For every harvested tree, the harvester

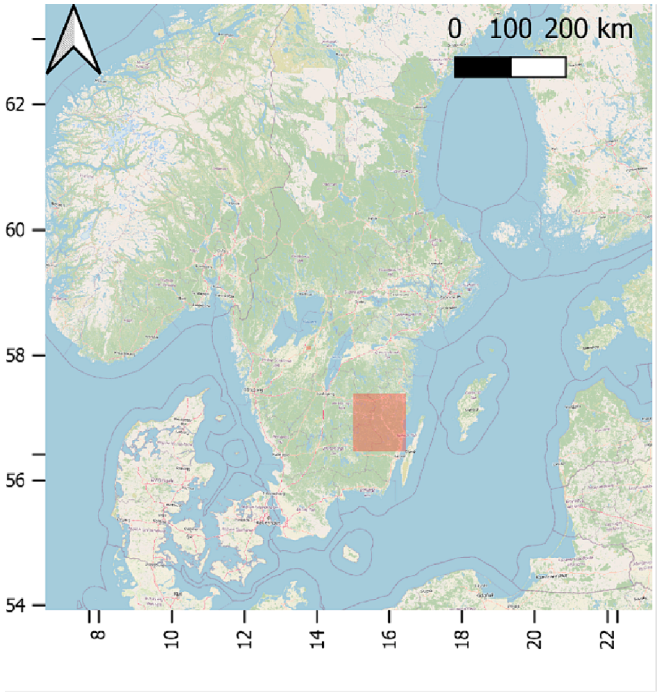

Fig. 1. Overview of southern Sweden with the study areas zoomed in (coordinates in WGS84; EPSG:4326).

registered tree species, diameter breast height (DBH), if it was bark beetle attacked or healthy (visually inspected by the harvester operator), the position of the harvester based on global navigation satellite system (GNSS), and the date of harvest. Since the harvester operator assessed the status of attacked or healthy trees, some trees in the green-attack phase were likely falsely assigned to the healthy class. National aerial *ortho*-photos (a mosaic with 0.16 m resolution) were provided in a web map service (WMS) from the Swedish National Land Survey, which were used to verify reported forest operations and for visual interpretation of the results.

2.2. Satellite data

The S2 images were selected using Google Earth Engine (GEE), from the data catalog "COPERNICUS/S2_SR", which provided Level 2 surface reflectance values. The S2 acquisitions covering the study area during 2018–2019 were filtered for cloud coverage < 20 % and visually inspected to identify useful scenes. Since no single scene in 2018 was cloud-free, we used GEE to derive a cloud-free mosaic based on the procedure of taking the median pixel value (in the time domain) per pixel, out of the useful scenes in each year, to derive a cloud-free mosaic. This approach enabled us to derive a "before attacks" image t1, based on the time range July 21 until August 31, 2018, which is within the vegetated season in the study area. Then, a single cloud-free image was identified on August 27, 2019 (Table 1), which was used as "after" image t2, although some trees attacked from a second swarming period – usually including a five-fold reduction of bark beetles compared to the main flight (Öhrn et al., 2014) – may still be in the green attack stage (Jactel et al., 2017). To investigate the temporal stability of ΔDRS from 2018 until different times in the season 2019, we derived cloud-free mosaics (as described above) based on four different time periods in 2019, spring ($t2_{*1}$), summer($t2_{*2}$), late summer ($t2_{*3}$), and autumn ($t2_{*4}$) – after the vegetation season (Table 1).

2.3. Rasterization of harvester reference data

The harvested tree positions were rasterized (10 × 10 m^2 pixels) to create heat maps of harvested trees for both attacked and healthy trees for each pixel. This enabled us to identify areas with different harvest intensities and derive the proportion of healthy and attacked harvested trees per pixel. The distribution of attacks per pixel was exponentially declining, with a range of 1 to 56. Most pixels had few attacks, and as the number of attacks per pixels increased, fewer pixels were available (Fig. 2). It is unlikely that as much as 56 trees were actually located within a single 10 × 10 m^2 pixel, but since the GNSS receiver was mounted on the harvester cabin roof and not on the harvester head, multiple records can have duplicated coordinates. The uncertainties in the harvester positioning may worsen this problem.

2.4. Derivation of DRS and ΔDRS

The DRS was derived as (cf. eq. (1) in Huo et al., 2021):

Table 1
Acquisition times of satellite images. The t2 images with names in subscript indicate the four different "after" images, which were used in the temporal stability analysis.

Dataset	Period	Purpose
DRS t1	21 Jul – 31 Aug 2018	before image for all ΔDRS analyses
DRS t2	27 Aug 2019	after image for main ΔDRS analysis
DRS $t2_{*1}$	30 Apr – 31 May 2019	after image 1 for seasonal stability analysis
DRS $t2_{*2}$	2 Jun – 20 Jul 2019	after image 2 for seasonal stability analysis
DRS $t2_{*3}$	27 Aug 2019	after image 3 for seasonal stability analysis
DRS $t2_{*4}$	21 Sep – 29 Oct 2019	after image 4 for seasonal stability analysis
DRS t3	25 Jun 2019	after image for clear-cut analysis

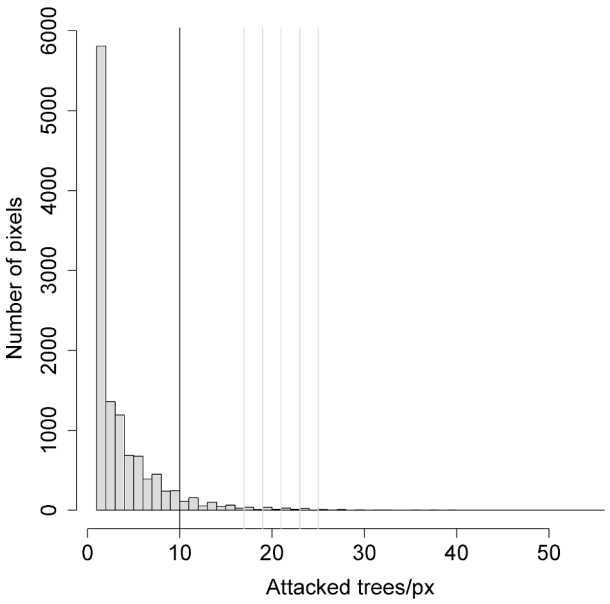

Fig. 2. Histogram of attacked trees per pixel. Vertical bar denotes truncation limit and gray vertical bars denote extended intervals.

$$DRS = \sqrt{Red^2 + SWIR^2} \quad (1)$$

using band 4 (10 × 10 m^2 pixels) as red, and band 12 (20 × 20 m^2 pixels) as SWIR. In Huo et al. (2021), the DRS was normalized with respect to the range of DRS values of spruce-dominated pixels and a threshold was estimated to separate healthy and attacked forest. The normalization reduces DRS changes due to phenology, enables comparisons of DRS between different seasons, and it is an efficient method for identifying attacked forest when we have a priori information that attacks do exist. However, in practice we may not have access to maps of spruce-dominated forest from sufficiently large areas to normalize and estimate the threshold accurately, and it could be more efficient to use the change of DRS over time. Therefore, this study tests the performance of using temporal DRS changes (ΔDRS) on mapping bark beetle damage. The assumption is that the tree species composition or vegetation in a pixel remains stable throughout the time span investigated with ΔDRS. Then, chlorophyll related changes (captured by the red band) and water induced changes (captured by the SWIR band) in the vegetation will be the main drivers of changing DRS values. Since the water exchange in vegetation is dependent on the phenology, we assumed that using approximately the same phenology season could ensure robust estimates. This was further investigated in Section 2.5.3 to explore the temporal stability of ΔDRS. We defined the ΔDRS as

$$\Delta DRS = DRS_{t2} - DRS_{t1} \quad (2)$$

using the image mosaic "after" as t2, and image mosaic "before" as t1. The ΔDRS pixel values for the single pixels or clusters of pixels were extracted and used to assess the usefulness in the following sections.

2.5. Analyses

2.5.1. Approach 1: Pixel level

The harvester data were used for two different validation approaches, one for the validation at pixel level and one for validation at cluster level. The harvester data after t2 (27. Aug 2019, Table 1) until the end of the year 2019 were used as references for the bark beetle mapping. In the first, we considered the number of attacked trees per pixel that could be detectable based on ΔDRS, hence indicate the relationship between the attack intensity and the ΔDRS. We extracted the

ΔDRS pixel values for the locations where the harvester had registered attacks. In each pixel interval with a width of 1 (applied to the range 1, 2, 3 … 56), we randomly put aside 10 % of the pixels for testing and used the other 90 % for modeling. Due to a lot of noise, the pixels for each interval were averaged to derive the mean ΔDRS value for each interval (separately for modeling and testing).

Müller et al., (2022) used similar harvester data, and they treated pixels with more than 10 registered trees as unreliable which were then removed. They did not explain the reasoning behind this, but bark beetles are more commonly attacking older and larger trees, >25 cm DBH as suggested by Sproull et al. (2015). By transferring this concept to a Swedish forest context (i.e., with smaller trees), we believe that this corresponds to trees with a DBH of about 20–40 cm in the managed forest in our study, which corresponds to a crown area of about 10–20 m^2 (Pretzsch et al., 2015). In case of a fully stocked, mature forest, there would only fit in about 5–10 trees in a single pixel (100 m^2). Hence, we agree with Müller et al., (2022) that it would only be somewhat reliable registrations within the range of about 1–10 trees per pixel.

The rasterized harvested tree map provided 11,786 pixels with at least one attacked spruce tree, 244 pixels with 10 attacks per pixel and at 17 attacks per pixel, we only had 24 pixels available (Fig. 2). For illustration purposes, we processed all our data, but for the higher values (e.g. 23 attacks/pixel), there were few or no pixels available. We therefore decided to widen the interval (over which the mean was computed) when there were fewer than 30 pixels, until at least 30 pixels were included (e.g. the interval was extended from [23,23] to [23,24] attacks/pixel, illustrated with gray vertical bars in Fig. 2). The limit of 30 pixels was selected as it corresponds to when a Student's t-distribution approximately converges into a normal distribution, but even if 30 pixels may be enough for the statistics, the mean value will be more accurate when computed from more pixels. There were only 747 pixels with more than 10 attacks/pixel (6 % of all pixels). Therefore, agreeing with the hypothesis by Müller et al., (2022), we also decided to truncate the dataset used for modeling at 10 trees per pixel (Fig. 2). We assumed a linear relationship between attacks and ΔDRS and estimated the model parameters with a linear regression model,

$$attacks = \alpha_0 + \alpha_1 \Delta DRS + \varepsilon \quad (3)$$

where *attacks* denote the number of attacked trees per pixel, ΔDRS the change of DRS, and ε is the residual standard error. The estimated parameters were $\alpha_0 = -4.844$, $\alpha_1 = 1316$, and $\varepsilon = 0.9077$. The regression model was used to predict the attacks of the validation dataset (the 10 % put aside) and the accuracy was estimated as root mean square error:

$$\mathrm{RMSE} = \sqrt{\frac{1}{n}\sum_{i=1}^{n}(\widehat{Y}_i - Y_i)^2} \quad (4)$$

with Y being the reference, $\widehat{Y}$ the prediction for i attacks/pixel, and n denoting the total number of intervals (10).

2.5.2. Approach 2: Cluster level

In the second validation approach, we created clusters of the attacked and healthy trees registered by the harvester, using the same period as for the single pixels (Fig. 3). The ΔDRS values of single pixels are not only decided by what happens within the single pixels but are also highly influenced by the surroundings. In particular, the SWIR band, which was only acquired at 20 × 20 m^2 pixels, was oversampled to enable deriving the DRS at 10 × 10 m^2 pixels. Therefore, the main difference here compared to the Approach 1: Pixel level, is that we studied clusters of pixels, instead of single pixels with a much larger variation. Assessing a slightly larger area (although small) reduces the impact of positioning errors and other noise we cannot control. To derive the clusters of attacked trees, we filtered the rasterized harvester pixels with the criteria that a single pixel should have > 5 trees and out of these, >50 % should be attacked. A closing morphological operation (dilation followed by erosion) was then applied using a 5 × 5 pixels kernel, implemented with the Whitebox plugin in QGIS (Lindsay, 2016), with the result that gaps smaller than 5x5 pixels were removed. The pixels fulfilling these criteria were then converted to polygons. A corresponding procedure was carried out to generate clusters with only healthy harvested trees. Then, we filtered the clusters and required them to be at least 30 m away from other clusters, and having a minimum area of 500 m^2. This generated 842 attacked tree clusters and 137 healthy tree clusters. The tree properties of the clustered datasets are presented in Table 2. The mean DBH of attacked clusters was 30.2 cm, while it was 27.8 cm for healthy clusters (Fig. 4), indicating similar tree properties in both groups. The significance was p < 2.2e-16, when comparing the two groups using a Kolmogorov-Smirnov test. However, the spread of DBH is a bit larger for the healthy trees (10.1 vs. 9.45 cm, Table 2).

Then, we extracted the mean, 1st, and 99th percentile of the ΔDRS pixel values for the clusters and used these as explanatory variables in a linear discriminant analysis (LDA, from the MASS package in R) to classify the ΔDRS clusters as healthy or attacked. To handle the class imbalance (842 attacked and 137 healthy clusters), we used all the healthy clusters but only a random sample (n = 137, using the function *sample* in R) of the attacked clusters to get a balanced dataset (n = 274) and hence enable a fair analysis. The accuracy was presented as a confusion matrix with the classifications and overall accuracy (OA).

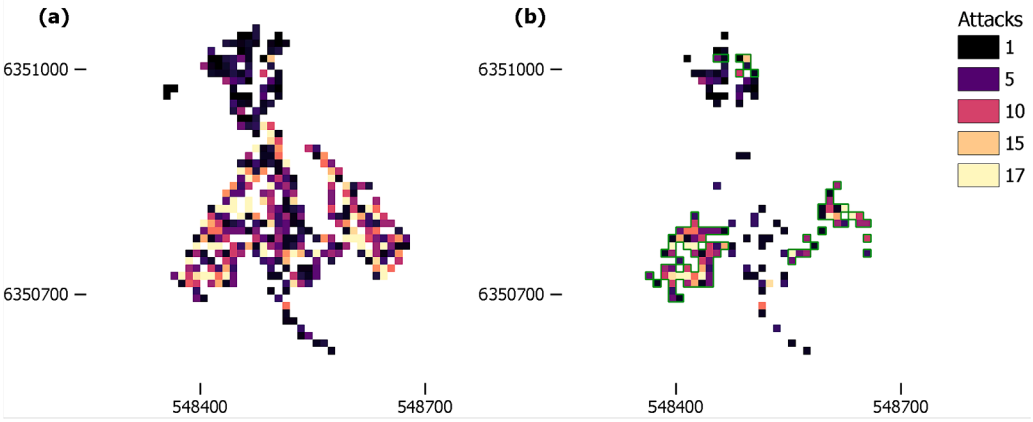

Fig. 3. Raster maps of trees registered by the harvester in EPSG:3006 – unit in meters. (a) Total number of trees registered by the harvester, rasterized to 10x10 m^2 pixels. (b) The same area filtered for the number of bark beetle killed trees (>5 cut trees in a pixel and more than 50 % of them being attacked). Delineation of clusters fulfilling the filter criteria in green. (For interpretation of the references to colour in this figure legend, the reader is referred to the web version of this article.)

Table 2
Properties of clustered polygons and the trees in these. D denote the diameter breast height.

Dataset	Mean Area (m^2)	Sd Area (m^2)	Min Area (m^2)	Max Area (m^2)	Mean D (cm)	Sd D (cm)	Min D (cm)	Max D (cm)	n
Healthy tree clusters	1,778	2,200	500	13,200	21.2	10.1	5.2	70.7	137
Attacked tree clusters	1,345	1,062	500	6,200	23.9	9.45	5.4	70.6	842
Clear-cuts	11,400	17,800	671	162,000	23.6	10.2	5.2	70.7	185

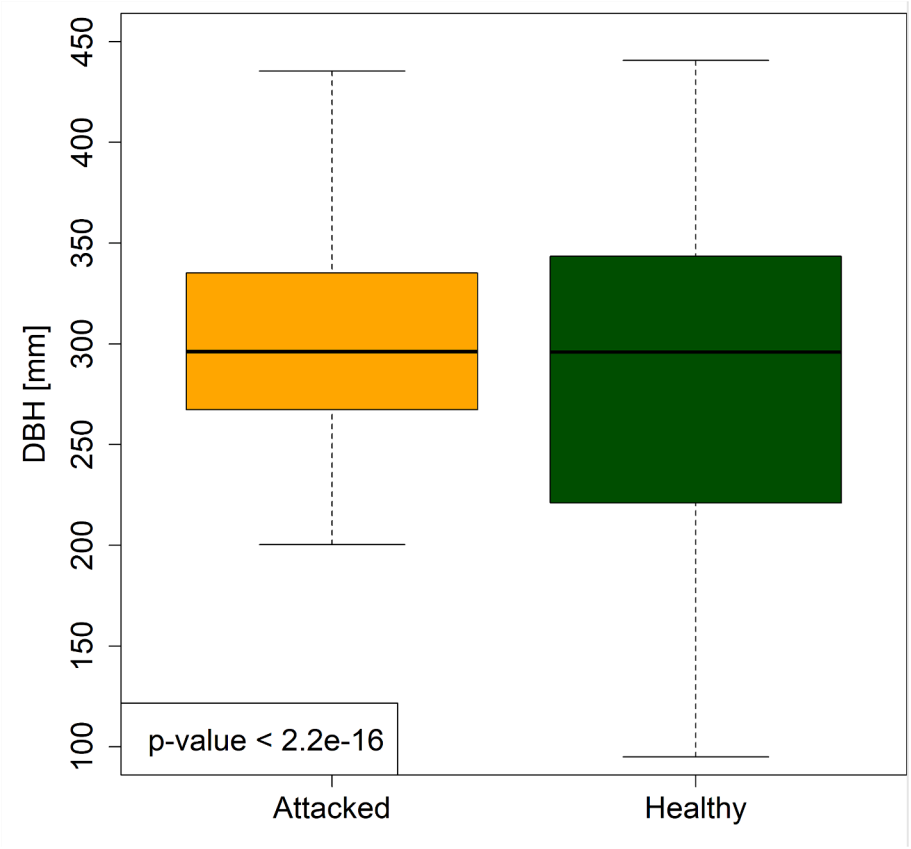

Fig. 4. Basal area-weighted diameter breast height of trees in the two cluster groups. The p-value represents the significance when comparing the two groups using a Kolmogorov-Smirnov test.

Clusters of clear-cuts were also derived using a corresponding approach, but including all harvested trees (more on the use of these in Section 2.5.3). These clusters were obtained using a buffer radius of 40 m and including at least 300 trees, harvested within the period from 1 Sep 2018, until 26 Aug 2019. Then, the clusters were visually inspected using aerial *ortho*-photographs from the Swedish Land Survey, captured in 2021–2022, and 13 stands were identified as outliers due to being only partly cut (e.g., due to thinning operations) or having false polygon borders (e.g., single trees were registered out on the road instead of in the forest, causing an overestimation of the polygon size). The automatically generated reference dataset included 185 clear-cuts harvested between the images t1 and t2 (Table 1), of which 13 were outliers. The properties of all the clear-cuts are described in Table 2 and these data will be further discussed in the Section 2.5.3.

2.5.3. *Other factors impacting ΔDRS*

In order to address our third objective, identify other useful experiences, we further identified factors that cause DRS changes and can potentially be misinterpreted as bark beetle attacks. By recognizing these cases, they can be managed with a greater attention and at best be masked out using auxiliary data. We focused on two additional contexts relevant for the forest sector: 1) how ΔDRS change due to various forest practices or other human induced activities – including commercial thinning, shelter wood cutting (even-aged harvesting where seed trees are left), and clear-cutting, and 2) the temporal stability of ΔDRS.

Most of the clear-cut clusters that were identified as outliers were in fact only partly cut stands, i.e., stands where commercial thinning had been applied (9), or cutting where seed trees were left (4). These clusters were not so many that a statistical validation could be used, but nevertheless – we visualize examples of these cases as indications on what can be expected. In Swedish forestry, commercial thinning involves a harvester cutting about 30–35 % of the basal area in order to increase the value of the remaining trees by improving the growing conditions through decreased competition. Even-aged harvesting methods can be carried out in different ways, but one common approach makes use of shelter wood cutting during the transition of two rotation periods and leaves seed trees for natural regeneration. It is often applied to pine dominated forest, and the largest trees are left in order to provide a natural seed source for the regeneration. Yet, the larger part of the forest is cut, although dominant trees are left – hence partly obstructing the spectral changes from the cutting. When the next generation of trees has started growing, the seed trees are cut as well. To test the accuracy of using ΔDRS to identify clear-cuts, we classified the ΔDRS map based on a threshold ($\Delta DRS \geq 0.06$) and assessed the accuracy with the 172 clear-

cut clusters (after the 13 outliers had been removed, Table 2). The threshold was subjectively chosen based on the ΔDRS values for the clear-cuts, visual interpretation of the ΔDRS raster, and comparisons with the harvested trees. The detection accuracy was expressed in percent of correctly classified clear-cut clusters.

The second context, temporal stability of ΔDRS, is an important aspect since cloud-free satellite images are often difficult to acquire the same time every year due to cloud cover (at least in Sweden). We hypothesized that the same phenological season should be used for the before and after images to enable confident conclusions based on ΔDRS. Nevertheless, optical satellite images may not be available due to cloud cover (as is often the case in Sweden), and then one may have to combine images from different seasons. Therefore, it is important to understand the robustness of ΔDRS to images from different seasons. We assessed this visually by deriving ΔDRS from the same *before attack image* (late summer 2018), but to different *after attack images*: spring, summer, late summer, and autumn (as defined in the study area in Sweden, the dates are shown in Table 1).

3. Results

3.1. Approach 1: Pixel level

The relationship between ΔDRS and number of attacks per pixel is illustrated in Fig. 5 a. This relationship is very noisy (remember the potential positing errors), and Fig. 5 b illustrates the corresponding relationship where the pixel values were averaged for each interval. Here, the relation shows a logarithmic growth from 0 up to about 17 attacks per pixel, then the spread increases drastically. Remembering that there were relatively few pixels available for more than 10 attacks/pixel, and that bark beetles usually attack mature forest, we disregarded the case with more than 10 attacks/pixel (Fig. 5 c).

The model results for prediction of the 10 % of the pixels that were put aside, was an RMSE = 2.95 attacks/pixel (53.6 %) and the linear model (Eq. (3) had an R^2 = 0.92. The predictions-vs-field plot is presented in Fig. 6. The variance around the 1:1 line is considerable, but the overall trend is yet linear. Despite a lot of noise in the overall relationship (Fig. 5 a), the tendency (Fig. 5 c) is that more intense attacks (in terms of number of infested/attacked trees) cause larger ΔDRS increases.

3.2. Approach 2: Cluster level

The second approach addressed healthy and attacked clusters of pixels. The group means were statistically different (using a one-sided *t*-test), with the 99th percentile of ΔDRS = 0.00104 for the healthy clusters and 0.0241 for the attacked clusters (Fig. 7). The Figs. 8-10 visualize a few different forest regions where the ΔDRS map is compared with *ortho*-photos, or overlaid with the number of attacked trees per pixel, as registered by a harvester after the ΔDRS (t1-t2). The classification assessment was expressed in a confusion matrix (Table 3), with healthy and attacked clusters predicted with an LDA. The accuracies ranged from 0.77 to 0.78 with the overall accuracy (OA) being 0.78 (Table 3). The figures confirm attacks predicted by the map, but they also visualize challenges with scattered harvester registrations, position inaccuracies, and possibly false positives of ΔDRS – which yet are impossible to test, since we are missing field data about the other areas indicated as attacked except where the harvesters have been.

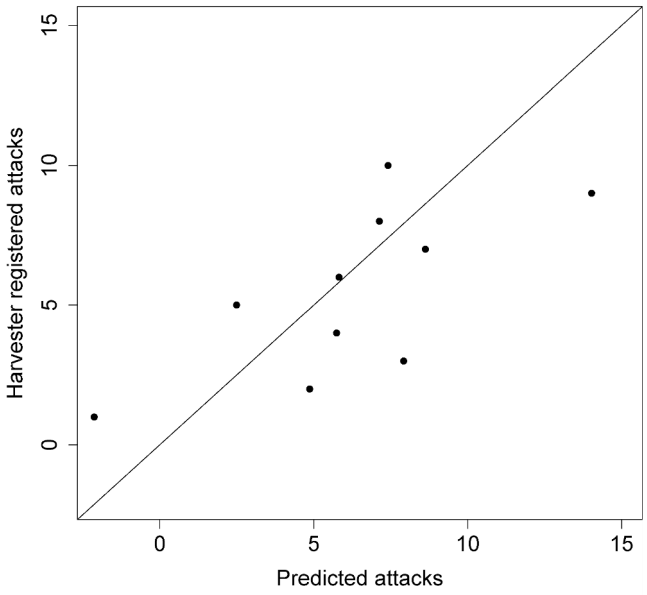

Fig. 6. Scatter-plot of predicted-vs-field registered attacks for the range of 1–10 attacks per pixel.

3.3. Other factors impacting ΔDRS

To generate a bark beetle map (e.g., as presence-absence) based on ΔDRS, we also need to address the cases when ΔDRS changes are driven by reasons other than the presence of bark beetle infested trees. We explored this in two contexts, where the first addressed the three forest management activities common in Swedish forestry: commercial thinning, shelter wood cutting (leaving seed trees), and clear-cuts. These actions are typically registered in databases and can hence normally be

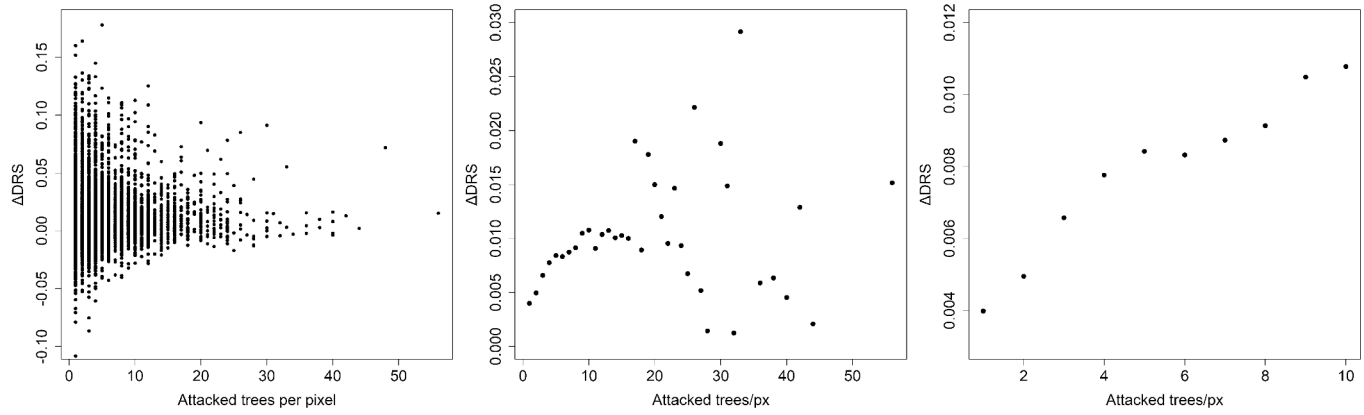

Fig. 5. a) ΔDRS vs. number of attacked trees per pixel. b) Grouped ΔDRS vs. number of attacked trees per pixel. c) The same scatterplot as (a) but only with 10 or fewer attacked trees per pixel.

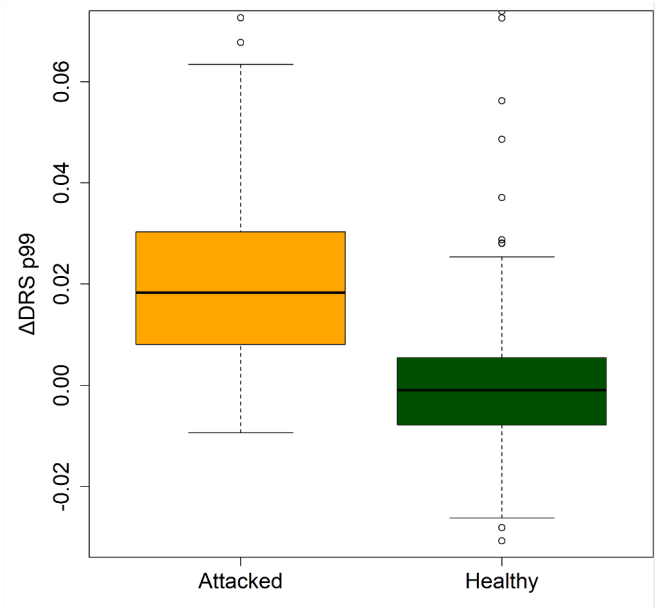

Fig. 7. Box plots of attacked and healthy cluster groups ΔDRS percentile 99 (p99) values used in the LDA.

masked out using these auxiliary data. Since we had too few occurrences for these contexts to enable a statistical evaluation, this section can only illustrate the problem as a qualitative assessment. Fig. 11 illustrates an area where commercial thinning (about 30–35 % of basal area removed) has been carried out and the change of ΔDRS was about 0.02 or below. Fig. 12 illustrates an area where most of the trees were cut, but the largest, dominant seed trees were left for regeneration. In this case, the loss was considerable and the ΔDRS values ranged about 0.05–0.06. An example of the third activity, a clear-cut, is illustrated in Fig. 13. For this clear-cut, the ΔDRS was about 0.06 or more for the pixels within the clear-cut, and lower at the edge pixels. Hence, ΔDRS appeared as a good clear-cut detector. The mean ΔDRS for all the clear-cut clusters was 0.126 while the pixels with the lowest 5 % ΔDRS within the clear-cuts had a change of 0.0638 and the 95 % change was 0.168 (Fig. 14). The quantitative assessment included a classification of the 172 clear-cuts, using 0.06 as threshold (Section 2.3, 2.5.3). Out of these, 100 % were correctly classified. Since the ΔDRS values for clear-cuts are significantly higher than areas of bark-beetle attacked trees, these can effectively be masked out.

The second context addressed the temporal stability of ΔDRS by using the same "before attack" image, but computing ΔDRS with respect to different "after attack" images throughout the season (Table 1). The effects of season are illustrated in Fig. 15, where it can be seen how larger changes (0.06 or more) are visible already in the spring (Fig. 15 a), but with large areas in-between ranging from 0 to 0.04, which later during the season stabilized and approached 0 (Fig. 15 b-d). We interpret this as the phenological changes driven by the internal water exchanges and chlorophyll shifts having a considerable impact and we therefore expect that the most reliable use of ΔDRS would be based on a "before" and "after" image from approximately the same day-of-year, but from different years.

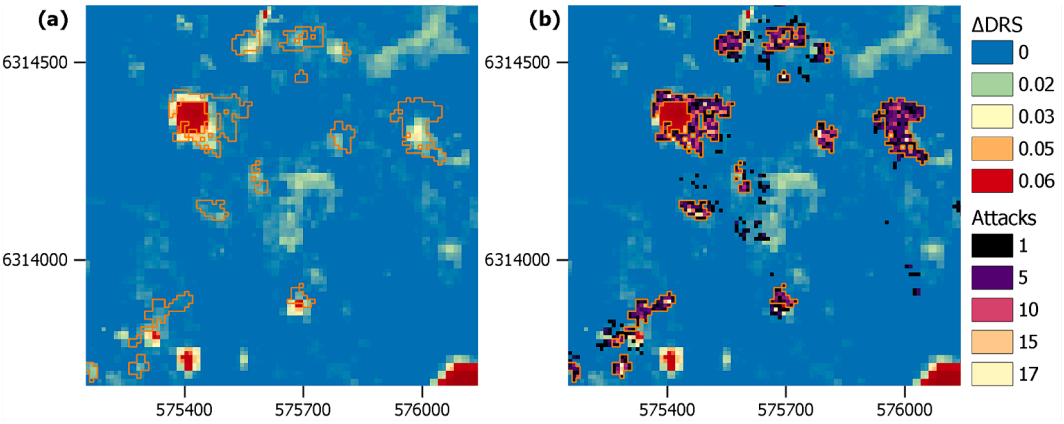

Fig. 8. a) Illustration of clusters (outlined in orange, representing pixels with more than 5 harvested trees – see 2.5.2), overlaying the ΔDRS map. b) The same area and maps in a), with the attacks registered. (For interpretation of the references to colour in this figure legend, the reader is referred to the web version of this article.)

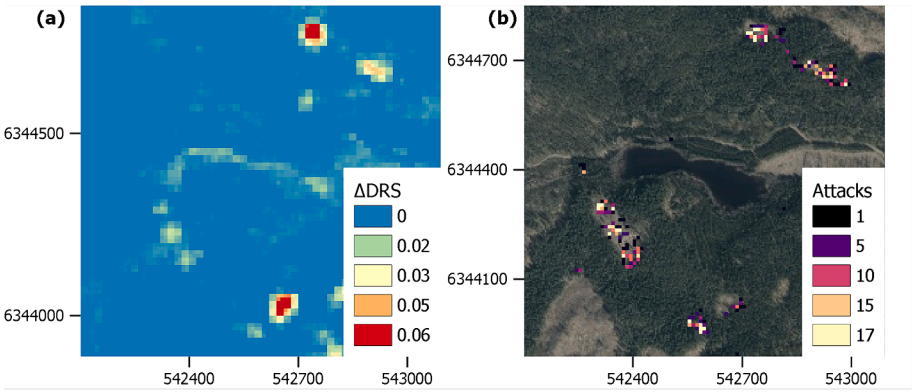

Fig. 9. Illustration of ΔDRS map (a) vs. *ortho*-photo (b) from 2022 with attacks registered by a harvester overlaid, coordinates in EPSG:3006.

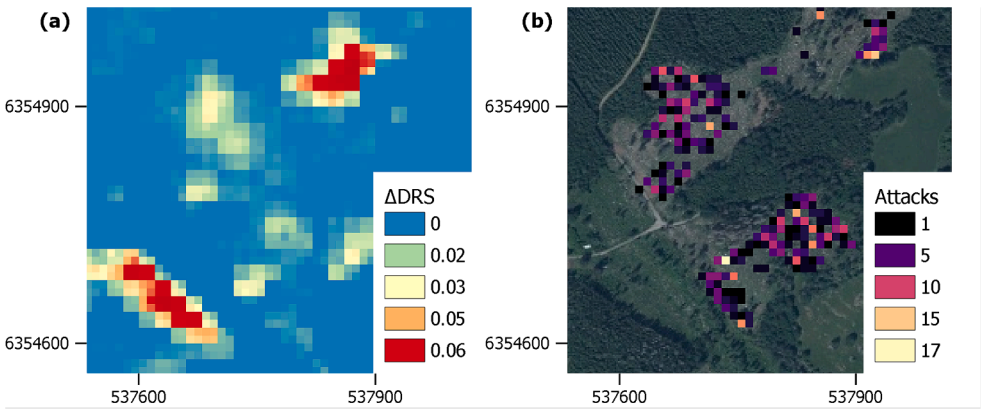

Fig. 10. Illustration of ΔDRS map (a) vs. *ortho*-photo (b) from 2022 with attacks registered by a harvester overlaid, coordinates in EPSG:3006.

Table 3
Confusion-matrix of healthy and attacked cluster predicted with LDA.

Pred \ Ref	Healthy	Attacked	Accuracy
Healthy	106	30	0.78 (precision)
Attacked	31	107	
Accuracy	0.78 (sensitivity)	0.77 (specificity)	**0.78 (overall)**

4. Discussion

A robust method for detecting bark beetle attacked forest over large areas is important to direct and plan efficient use of management resources as early as possible, e.g., to refine the timber value while it is still possible. This study has presented analyses that show that the use of the new ΔDRS index, based on S2 images, can contribute to such mapping applicable to, e.g., detecting forest damage and risk assessments across time and space. It uses the high sensitivity to bark beetle infested forests observed in bands 4 and 12 of S2 images, as demonstrated in (Huo et al., 2021), and avoids the need for information on the species composition of the forest. The overall relationship of single pixels, although noisy, showed that higher ΔDRS changes indicated more bark beetle attacked trees. The OA classification accuracy of 0.78 at the cluster level is better than, or of the same order, as has been reported with other indices tested on balanced datasets. For example, Dalponte

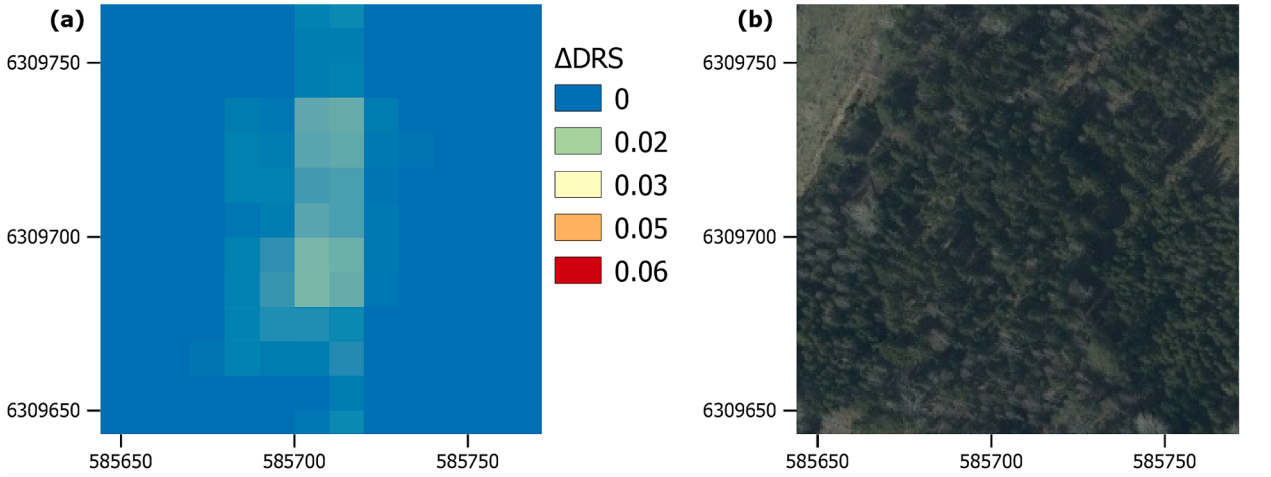

Fig. 11. Illustration of an area affected by commercial thinning, coordinates EPSG:3006. a) ΔDRS 2018–2019, b) *ortho*-photo 2021.

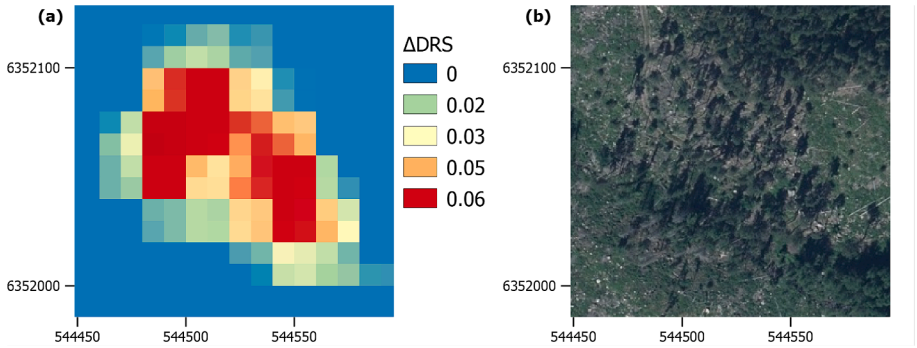

Fig. 12. Illustration of an even aged managed forest that was harvested but letting seed trees remain. Coordinates in EPSG:3006. a) ΔDRS, b) *ortho*-photo 2021.

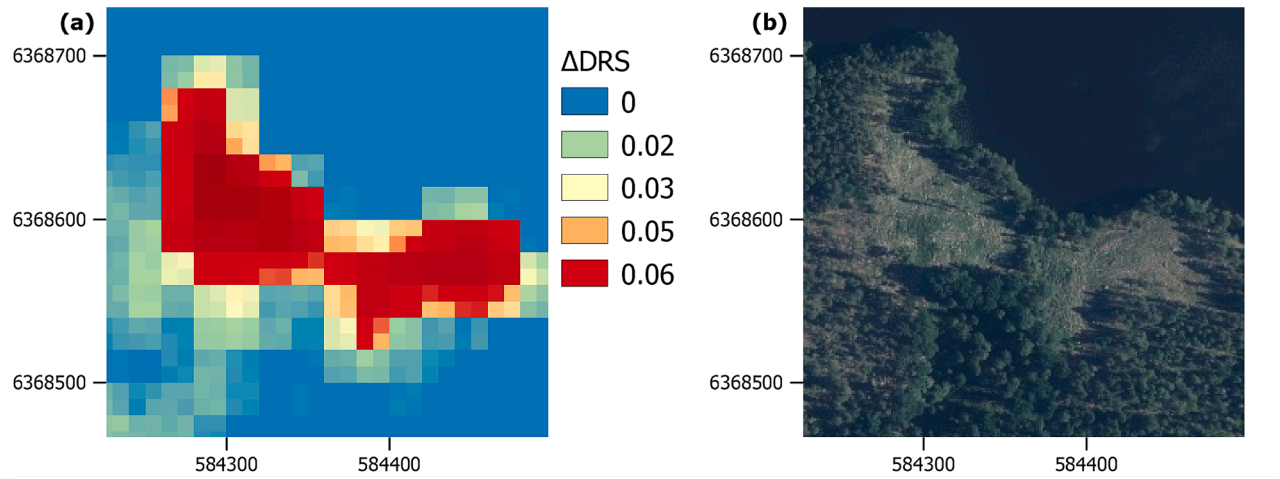

Fig. 13. Coordinates in EPSG:3006. a) ΔDRS with clear-cuts identified as red. b) Ortho-photo 2022. (For interpretation of the references to colour in this figure legend, the reader is referred to the web version of this article.)

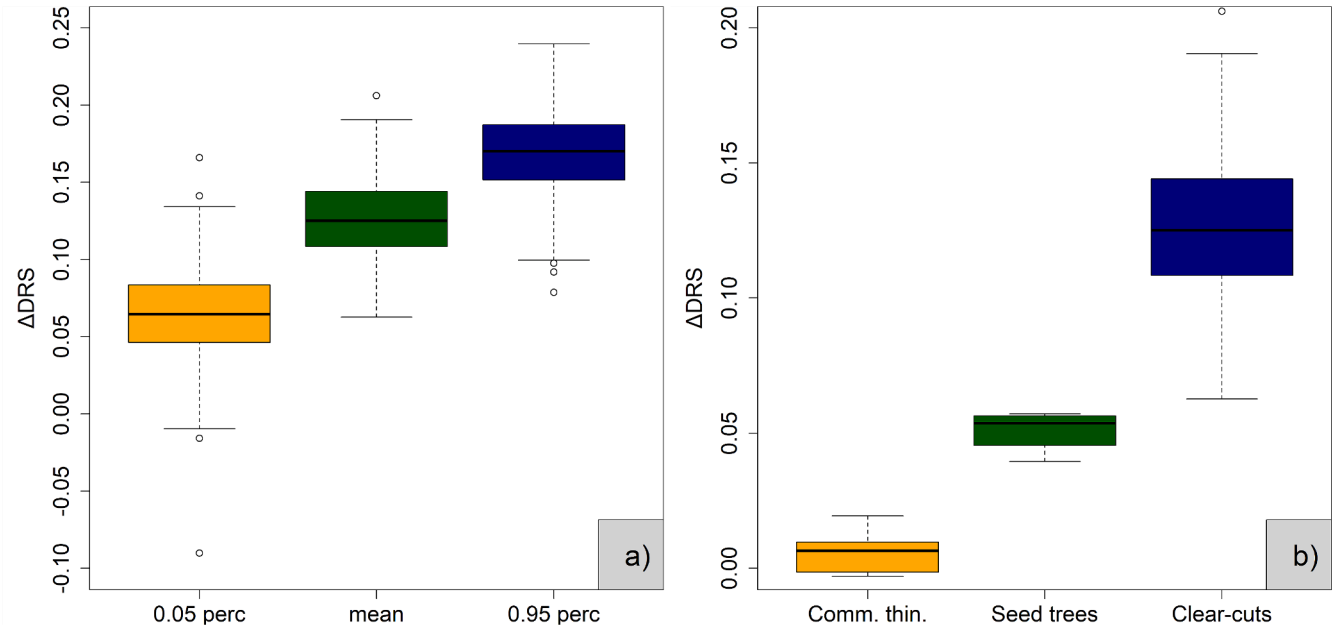

Fig. 14. Boxplots of ΔDRS values for a) the clear-cut clusters. 5th percentile (orange), mean (green), 95th percentile (blue) b) the mean ΔDRS for the three groups of other factors, commercial thinning, seed trees, and clear-cuts. (For interpretation of the references to colour in this figure legend, the reader is referred to the web version of this article.)

et al., 2022 showed a best case with 0.73, but most combinations were about 0.7 or lower. It is higher than Tanase et al. (2018) who reported (64–74 %) when using L-band SAR at a test site in Germany and higher than Bozzini et al. (2023) who reported (58–72 %) when using vegetation indices from S2 in an alpine region in Italy. It is similar to the results from Gao (2022) who reported a classification accuracy of 0.72–0.8, when using hyperspectral reflectance and machine learning models in China. At the same time, we want to stress that comparisons of results across studies are difficult due to, e.g., various study designs, spatial scales, resolutions, datasets, and times after attack, to mention a few factors. The OA was similar or slightly lower than we reported using NDRS in a case study at a small Swedish test site (0.8–0.9, Huo et al., 2021). Yet, these results together with the other analyses show that the method can be useful for large area mapping and an operational context. Furthermore, the potential impacts of the work are considerable, e.g., when used for national damage maps, resource maps for risk analyses (for the coming years), as input data to studies on environmental and structural factors and their associations with bark beetle damage and forest susceptibility, etc. The practical aspect that changes captured through ΔDRS are assumed to reflect chlorophyll and water induced changes in the vegetation, i.e., due to bark beetles or other disturbances, is straightforward without requirements on knowing the species composition (as is the case for the NDRS). Hence, all tree species compositions present in the landscape were included in our study.

The use of operational harvester data explored in this study has been a unique possibility of using a very large amount of field reference trees from a large spatial area. Nevertheless, practical uncertainties related to the reference data as well as those related to the satellite data have partly obstructed clear, convincing results. Since the tree status (attacked or healthy) was assigned by the harvester operator, trees in the green attack phase were probably not assigned as attacked in the reference data, and hence not classified as such. The challenges of not having a well-designed experiment in advance reduced the statistical possibilities to draw conclusions, e.g., due to class imbalances of

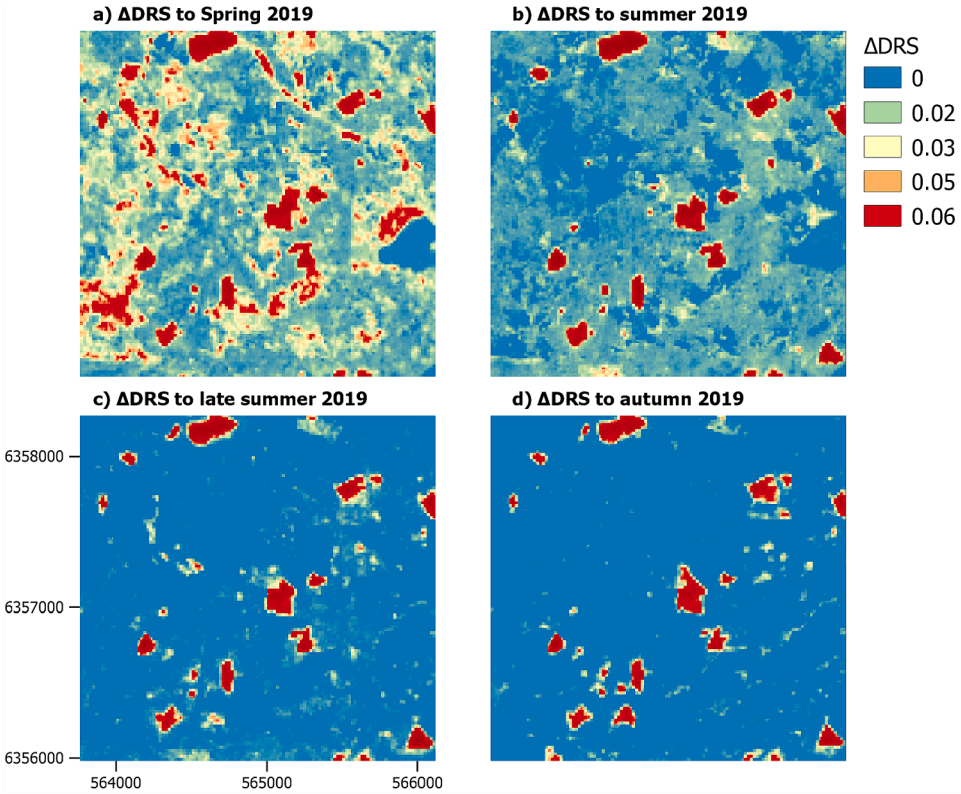

Fig. 15. The temporal stability of the ΔDRS, as computed from the same "before attack" image, but until different "after attack" images (Table 1) the following year: a) spring, b) summer, c) late summer, d) autumn. Coordinates in EPSG:3006.

attacks/healthy trees, insufficient number of attacked trees within the spatial resolution of the S2 satellite sensor, and location uncertainties related both to the harvester and to satellite data, to mention a few. Furthermore, the spatial resolution was different for the red and shortwave infrared bands (4 and 12) used to compute ΔDRS (Clerc and Team, 2022), which influences the estimates of single pixels.

Based on the results of the first, pixel-level approach, we could identify a linear relationship between the ΔDRS index and the intensity of bark beetle attacks. We avoided testing the relationship above 10 attacks/pixel, due to the unreliable registrations, which was further confirmed in the scatter plot (Fig. 5 b). The prediction uncertainty of single pixels was considerable and one possible reason (acknowledged also by Müller et al., 2022) was the positional inaccuracy of the bark beetle trees registered by the harvester, since the GNSS receiver was located on the harvester cabin roof rather than on the harvester head. Furthermore, the positional inaccuracies of GNSS receivers within the forest can be significant, although they have decreased in recent years thanks to their improved abilities of using multiple GNSSs (Hauglin et al., 2017; Næsset and Gjevestad, 2008; Noordermeer et al., 2021; Persson et al., 2022; Valbuena et al., 2010). Additionally, the location accuracy of the satellite pixels is about 11 m (~1 pixel) for unrefined S2 images (Clerc and Team, 2022), which contributes to the spatial disparity between harvest and S2 data.

Other reasons may be trees being in the green-attack phase, i.e., at an infestation stage with no visible discoloration of the tree crowns and thus it is challenging to detect these in S2 images. The spectral changes can be seen at the earliest 7–8 weeks after attacks using multispectral drone imagery, reported by Huo et al., (2023). Hence, there may be attacked trees that do not show any spectral changes at the time for the acquisition of the satellite image (hence affecting the ΔDRS), although the harvester operator may have easily seen the spectral changes of the canopy later in the fall, at the time these trees were harvested.

As an attempt to reduce the impact of location-related inaccuracies, the second approach analyzed clusters of attacked trees. Using the smallest area limit of 500 m^2, we had at least five pixels for each cluster, which therefore stabilized spectral inaccuracies of the single pixels. The clusters were generated automatically based on the harvester registrations, and based on the visual interpretation, we still think that the delineation step can be improved. As we are not aware of any operational large-area mappings wall-to-wall today, the OA of 0.78 at cluster-level for our method appears useful, given the spatial scale of the sensors and the study area. The spatial resolution of the satellite images was rather coarse and it is rare that most trees within a pixel would be attacked. Huo et al., 2021 suggested that at least half of the trees within a pixel need to be attacked to be visible in S2. Furthermore, except for Müller et al., (2022) and Jamali et al., (2023), we are not aware of any other research that have used operational harvester data for wall-to-wall mapping of the European spruce bark beetle at this spatial scale and resolution.

The ΔDRS index has the potential to reflect many forest changes related to chlorophyll and water changes. These include, e.g., 1) natural disturbances such as forest insect infestation, disease infection, storm damage, drought, haze, wildlife damage etc., 2) human induced changes, e.g., forest management actions, and 3) seasonal changes, e.g., phenology. We acknowledge that without appropriate masking, all the cases affecting ΔDRS could cause false positives in a bark beetle map and, e.g., by using auxiliary data about forest management activities, such ambiguities can be reduced. Detection of forest operations (i.e., harvesting and thinning) has been demonstrated with optical satellite images, relying on similar wavelength regions as used in the DRS. For example, the red, near-infrared, and shortwave-infrared bands have been used in Landsat images (Heikkonen and Varjo, 2004; Olsson, 1994; Schroeder et al., 2011). Similarly, the near-infrared and mid-infrared bands have been used in SPOT-4 images (Magnusson et al., 2008), and the red-edge and shortwave-infrared bands have been used as well as the normalized difference vegetation index in Sentinel-2 images (Abdi,

2020; López-Amoedo et al., 2021). For longer time intervals, the Harmonized Landsat Sentinel-2 product has been used with the normalized burned ratio derived from the near-infrared and shortwave-infrared bands (Mulverhill et al., 2023). The third section of our analyses addressed the forest management actions and phenology (i.e., temporal changes throughout the year). In particular, commercial thinning caused ΔDRS changes that were similar to bark beetle attacks, while the harvested areas with seed trees left had a ΔDRS somewhere between thinned and clear-cut forest, hence a bit higher ΔDRS (around 0.04–0.06). However, masking only based on ΔDRS values in this range could cause intense bark beetle outbreaks to be falsely masked. The clear-cuts had a mean ΔDRS higher than 0.06 and all clear-cuts were correctly classified (using a threshold of 0.06). Therefore, clear-cuts can be identified and masked from a ΔDRS map indicating bark beetle damage. In the time series (Fig. 15), the clear-cuts appeared visible during all seasons, hence being less sensitive to the more restrictive conditions for which ΔDRS may be used in order to represent bark beetle attacks.

As a further tool to discriminate damage types (or factors) causing ΔDRS changes, it could be possible to use more frequent observations or longer time series. For example, bark beetle damage is often visible in S2 images from August to October, so ΔDRS changes in this period may largely be caused by bark beetle infestations, while ΔDRS changes during the summer may be related to drought, and changes during the winter may be caused by storms (common in Sweden). Moreover, the spatial pattern in moving windows can be useful to identify bark beetle damage (Olsson et al., 2023). To date, we are not aware of any studies able to distinguish the damage types and it would therefore be a meaningful future work. This study also showed how forest management activities can be mapped with ΔDRS and how they potentially influence the mapping accuracy of bark beetle damages.

The ΔDRS changes caused by phenology was not extensively explored in this study. Yet, we interpreted areas with a deviating ΔDRS in the early season and almost no difference (approaching zero) later, as phenological changes driven by the internal water exchanges and chlorophyll shifts having a considerable impact. Therefore, for mapping purposes we suggest using maps from similar seasons (day-of-year) to calculate the ΔDRS, otherwise a seasonal time-series analysis would be needed.

We have not touched upon the topic of early detection. Nevertheless, we suggest that a near-real time mapping could potentially be developed by continuously deriving sequential ΔDRS maps, e.g., every month (using the current month as "after" image, and comparing with an image one year ago). Then, the phenological impacts that were demonstrated in Fig. 15 could be reduced and the larger changes could effectively be masked/identified. This would release resources to carefully handle cases with smaller ΔDRS values, i.e., in the range of 0 to 0.03, where bark beetle attacks would typically appear. Nevertheless, the near-real-time mapping refers to the time when we can obtain maps, instead of the time when the attacks happen. So far, no research has shown an acceptable accuracy on detecting green-attack trees with S2 images.

5. Conclusions

This study demonstrated how S2 satellite images could be used to compute a new ΔDRS index related to bark beetle attacked forest. The index map was validated with reference trees registered by operational harvesters, although many issues related to position accuracy and spatial resolution of S2 images reduced the most convincing results. To reduce such issues, automatic clusters of healthy and attacked trees were derived, for which the mean ΔDRS was extracted and used to predict healthy or attacked clusters using LDA. This assessment showed an overall accuracy of 0.78 and that the attacked tree clusters in our study on average had a ΔDRS of 0.02. When ΔDRS changes were larger, in particular above 0.06, they indicated clear-cut forest. An assessment of 172 clear-cut clusters were predicted with 100 % accuracy, using this criterion. Smaller changes such as thinning or partial cutting were also reflected in the ΔDRS, although smaller than for clear-cut forest. We suggest masking such areas using auxiliary data about forest management activities. We conclude that ΔDRS is useful in mapping chlorophyll and water related changes such as disturbances (bark beetle attacked forest in our case) and management operations, but it is also very suitable for clear cut mapping.

CRediT authorship contribution statement

Henrik J. Persson: Writing – review & editing, Writing – original draft, Visualization, Validation, Methodology, Investigation, Funding acquisition, Formal analysis, Data curation, Conceptualization. **Simon Kärvemo:** Writing – review & editing, Writing – original draft, Funding acquisition. **Eva Lindberg:** Writing – review & editing, Writing – original draft, Funding acquisition. **Langning Huo:** Writing – review & editing, Writing – original draft, Project administration, Methodology, Data curation.

Declaration of competing interest

The authors declare that they have no known competing financial interests or personal relationships that could have appeared to influence the work reported in this paper.

Data availability

Data will be made available on request.

Acknowledgments

We thank the Hildur & Sven Wingquist's Foundation for Forest Research, Nils and Dorthi Troedsson's Foundation, the Seydlitz Foundation, Brattåsstiftelsen F20:02, Skogssällskapet 2020-774, and Formas – a Swedish Research Council for Sustainable Development 2021-01610 for financial support that has enabled this study. We also thank the anonymous reviewers that helped us improving the manuscript.

References

Abdi, A.M., 2020. Land cover and land use classification performance of machine learning algorithms in a boreal landscape using Sentinel-2 data. Giscience Remote Sens. 57, 1–20. https://doi.org/10.1080/15481603.2019.1650447.

Abdullah, H., Skidmore, A.K., Darvishzadeh, R., Heurich, M., 2019. Timing of red-edge and shortwave infrared reflectance critical for early stress detection induced by bark beetle (Ips typographus, L.) attack. Int. J. Appl. Earth Obs. Geoinf. 82, 101900 https://doi.org/10.1016/j.jag.2019.101900.

Bárta, V., Lukeš, P., Homolová, L., 2021. Early detection of bark beetle infestation in Norway spruce forests of Central Europe using Sentinel-2. Int. J. Appl. Earth Obs. Geoinf. 100 https://doi.org/10.1016/j.jag.2021.102335.

Bárta, V., Hanuš, J., Dobrovolný, L., Homolová, L., 2022. Comparison of field survey and remote sensing techniques for detection of bark beetle-infested trees. For. Ecol. Manage. 506 https://doi.org/10.1016/j.foreco.2021.119984.

Bozzini, A., Francini, S., Chirici, G., Battisti, A., Faccoli, M., 2023. Spruce Bark Beetle Outbreak Prediction through Automatic Classification of Sentinel-2 Imagery. Forests 14, 1116. https://doi.org/10.3390/f14061116.

Candotti, A., De Giglio, M., Dubbini, M., Tomelleri, E., 2022. A Sentinel-2 Based Multi-Temporal Monitoring Framework for Wind and Bark Beetle Detection and Damage Mapping. Remote Sens. 14, 1–29. https://doi.org/10.3390/rs14236105.

Clerc, S., Team, M., 2022. S2-PDGS-MPC-DQR.

Dalponte, M., Solano-Correa, Y.T., Frizzera, L., Gianelle, D., 2022. Mapping a European Spruce Bark Beetle Outbreak Using Sentinel-2 Remote Sensing Data. Remote Sens. 14 https://doi.org/10.3390/rs14133135.

Estrada, J.S., Fuentes, A., Reszka, P., Auat Cheein, F., 2023. Machine learning assisted remote forestry health assessment: a comprehensive state of the art review. Front. Plant Sci. 14, 1–25. https://doi.org/10.3389/fpls.2023.1139232.

Gao, B., Yu, L., Ren, L., Zhan, Z., Luo, Y., 2022. Early Detection of Dendroctonus valens Infestation with Machine Learning Algorithms Based on Hyperspectral Reflectance. Remote Sens. 14, 1–16. https://doi.org/10.3390/rs14061373.

Hanewinkel, M., Breidenbach, J., Neeff, T., Hanewinkel, E.K.M., 2008. Seventy-seven years of natural disturbances in a mountain forest area - The influence of storm, snow, and insect damage analysed with a long-term time series. Can. J. for. Res. 38, 2249–2261. https://doi.org/10.1139/X08-070.

Hauglin, M., Hansen, E.H., Næsset, E., Busterud, B.E., Gjevestad, J.G.O., Gobakken, T., 2017. Accurate single-tree positions from a harvester: a test of two global satellite-

based positioning systems. Scand. J. for. Res. 32, 774–781. https://doi.org/10.1080/02827581.2017.1296967.
Hedgren, P.O., Schroeder, L.M., Weslien, J., 2003. Tree killing by Ips typographus (Coleoptera: Scolytidae) at stand edges with and without colonized felled spruce trees. Agric. for. Entomol. 5, 67–74. https://doi.org/10.1046/j.1461-9563.2003.00164.x.
Heikkonen, J., Varjo, J., 2004. Features : A Comparison of Different Classifiers in Boreal Forest Conditions. For. Sci. 50, 579–588.
Hlásny, T., Zimová, S., Merganičová, K., Štěpánek, P., Modlinger, R., Turčáni, M., 2021. Devastating outbreak of bark beetles in the Czech Republic: Drivers, impacts, and management implications. For. Ecol. Manage. 490 https://doi.org/10.1016/j.foreco.2021.119075.
Huo, L., Persson, H.J., Lindberg, E., 2021. Early detection of forest stress from European spruce bark beetle attack, and a new vegetation index: Normalized distance red & SWIR (NDRS). Remote Sens. Environ. 255, 1–18. https://doi.org/10.1016/j.rse.2020.112240.
Huo, L., Lindberg, E., Bohlin, J., Persson, H.J., 2023. Assessing the detectability of European spruce bark beetle green attack in multispectral drone images with high spatial- and temporal resolutions. Remote Sens. Environ. 287, 113484 https://doi.org/10.1016/j.rse.2023.113484.
Jactel, H., Bauhus, J., Boberg, J., Bonal, D., Castagneyrol, B., Gardiner, B., Gonzalez-Olabarria, J.R., Koricheva, J., Meurisse, N., Brockerhoff, E.G., 2017. Tree Diversity Drives Forest Stand Resistance to Natural Disturbances. Curr. for. Reports 3, 223–243. https://doi.org/10.1007/s40725-017-0064-1.
Jamali, S., Olsson, P.O., Ghorbanian, A., Müller, M., 2023. Examining the potential for early detection of spruce bark beetle attacks using multi-temporal Sentinel-2 and harvester data. ISPRS J. Photogramm. Remote Sens. 205, 352–366. https://doi.org/10.1016/j.isprsjprs.2023.10.013.
Kärvemo, S., Van Boeckel, T.P., Gilbert, M., Grégoire, J.C., Schroeder, M., 2014. Large-scale risk mapping of an eruptive bark beetle - Importance of forest susceptibility and beetle pressure. For. Ecol. Manage. 318, 158–166. https://doi.org/10.1016/j.foreco.2014.01.025.
Kärvemo, S., Johansson, V., Schroeder, M., Ranius, T., 2016. Local colonization-extinction dynamics of a tree-killing bark beetle during a large-scale outbreak. Ecosphere 7, 1–14. https://doi.org/10.1002/ecs2.1257.
Kautz, M., 2014. On correcting the time-lag bias in aerial-surveyed bark beetle infestation data. For. Ecol. Manage. 326, 157–162. https://doi.org/10.1016/j.foreco.2014.04.010.
Kautz, M., Schopf, R., Ohser, J., 2013. The "sun-effect": Microclimatic alterations predispose forest edges to bark beetle infestations. Eur. J. for. Res. 132, 453–465. https://doi.org/10.1007/s10342-013-0685-2.
Lindsay, J.B., 2016. Whitebox GAT: A case study in geomorphometric analysis. Comput. Geosci. 95, 75–84.
López-Amoedo, A., Álvarez, X., Lorenzo, H., Rodríguez, J.L., 2021. Multi-temporal sentinel-2 data analysis for smallholding forest cut control. Remote Sens. 13, 1–32. https://doi.org/10.3390/rs13152983.
Luo, Y., Huang, H., Roques, A., 2023. Early Monitoring of Forest Wood-Boring Pests with Remote Sensing. Annu. Rev. Entomol. 68, 277–298. https://doi.org/10.1146/annurev-ento-120220-125410.
Magnusson, M., Fransson, J.E.S., Olsson, H., 2008. Change detection of thinned Norway spruce stands using optical SPOT-4 satellite data. Can. J. Remote Sens. 34, 431–437. https://doi.org/10.5589/m08-035.
Mandl, L., Lang, S., 2023. Uncovering Early Traces of Bark Beetle Induced Forest Stress via Semantically Enriched Sentinel-2 Data and Spectral Indices. PFG -. J. Photogramm. Remote Sens. Geoinf. Sci. 91, 211–231. https://doi.org/10.1007/s41064-023-00240-4.
Müller, M., Olsson, P.O., Eklundh, L., Jamali, S., Ardö, J., 2022. Features predisposing forest to bark beetle outbreaks and their dynamics during drought. For. Ecol. Manage. 523 https://doi.org/10.1016/j.foreco.2022.120480.
Mulverhill, C., Coops, N.C., Achim, A., 2023. Continuous monitoring and sub-annual change detection in high-latitude forests using Harmonized Landsat Sentinel-2 data. ISPRS J. Photogramm. Remote Sens. 197, 309–319. https://doi.org/10.1016/j.isprsjprs.2023.02.002.
Næsset, E., Gjevestad, J.G., 2008. Performance of GPS precise point positioning under conifer forest canopies. Photogramm. Eng. Remote Sensing 74, 661–668. https://doi.org/10.14358/PERS.74.5.661.
Noordermeer, L., Sørngård, E., Astrup, R., Næsset, E., Gobakken, T., 2021. Coupling a differential global navigation satellite system to a cut-to-length harvester operating system enables precise positioning of harvested trees. Int. J. for. Eng. 32, 119–127. https://doi.org/10.1080/14942119.2021.1899686.
Öhrn, P., Långström, B., Lindelöw, Å., Björklund, N., 2014. Seasonal flight patterns of Ips typographus in southern Sweden and thermal sums required for emergence. Agric. for. Entomol. 16, 147–157. https://doi.org/10.1111/afe.12044.
Olsson, H., 1994. Changes in satellite-measured reflectances caused by thinning cuttings in Boreal forest. Remote Sens. Environ. 50, 221–230. https://doi.org/10.1016/0034-4257(94)90072-8.
Olsson, P.-O., Bergman, H., Piltz, K., 2023. Exploring the potential to use in-between pixel variability for early detection of bark beetle attacked trees. Agil. Giscience Ser. 4, 1–6. https://doi.org/10.5194/agile-giss-4-35-2023.
Ortiz, S.M., Breidenbach, J., Kändler, G., 2013. Early detection of bark beetle green attack using terraSAR-X and rapideye data. Remote Sens. 5, 1912–1931. https://doi.org/10.3390/rs5041912.
Pasztor, F., Matulla, C., Rammer, W., Lexer, M.J., 2014. Drivers of the bark beetle disturbance regime in Alpine forests in Austria. For. Ecol. Manage. 318, 349–358. https://doi.org/10.1016/j.foreco.2014.01.044.
Patacca, M., Lindner, M., Lucas-Borja, M.E., Cordonnier, T., Fidej, G., Gardiner, B., Hauf, Y., Jasinevičius, G., Labonne, S., Linkevičius, E., Mahnken, M., Milanovic, S., Nabuurs, G.J., Nagel, T.A., Nikinmaa, L., Panyatov, M., Bercak, R., Seidl, R., Ostrogović Sever, M.Z., Socha, J., Thom, D., Vuletic, D., Zudin, S., Schelhaas, M.J., 2023. Significant increase in natural disturbance impacts on European forests since 1950. Glob. Chang. Biol. 29, 1359–1376. https://doi.org/10.1111/gcb.16531.
Persson, H.J., Ekström, M., Ståhl, G., 2022. Quantify and account for field reference errors in forest remote sensing studies. Remote Sens. Environ. 283, 19. https://doi.org/10.1016/j.rse.2022.113302.
Potterf, M.C.N., Kočická, E., Ferenčík, J., Mezei, P., Jakuš, R., 2019. Landscape-level spread of beetle infestations from windthrown- and beetle-killed trees in the non-intervention zone of the Tatra National Park, Slovakia (Central Europe). For. Ecol. Manage. 432, 489–500.
Pretzsch, H., Biber, P., Uhl, E., Dahlhausen, J., Rötzer, T., Caldentey, J., Koike, T., van Con, T., Chavanne, A., Seifert, T., du Toit, B., Farnden, C., Pauleit, S., 2015. Crown size and growing space requirement of common tree species in urban centres, parks, and forests. Urban for. Urban Green. 14, 466–479. https://doi.org/10.1016/j.ufug.2015.04.006.
Raffa, K.F., Aukema, B.H., Bentz, B.J., Carroll, A.L., Hicke, J.A., Kolb, T.E., 2015. Responses of tree-killing bark beetles to a changing climate. In: Climate Change and Insect Pests. CABI, Wallingford UK, pp. 173–201.
Rousi, E., Fink, A.H., Andersen, L.S., Becker, F.N., Beobide-Arsuaga, G., Breil, M., Cozzi, G., Heinke, J., Jach, L., Niermann, D., Petrovic, D., Richling, A., Riebold, J., Steidl, S., Suarez-Gutierrez, L., Tradowsky, J.S., Coumou, D., Düsterhus, A., Ellsäßer, F., Fragkoulidis, G., Gliksman, D., Handorf, D., Haustein, K., Kornhuber, K., Kunstmann, H., Pinto, J.G., Warrach-Sagi, K., Xoplaki, E., 2023. The extremely hot and dry 2018 summer in central and northern Europe from a multi-faceted weather and climate perspective. Nat. Hazards Earth Syst. Sci. 23, 1699–1718. https://doi.org/10.5194/nhess-23-1699-2023.
Schroeder, T.A., Wulder, M.A., Healey, S.P., Moisen, G.G., 2011. Mapping wildfire and clearcut harvest disturbances in boreal forests with Landsat time series data. Remote Sens. Environ. 115, 1421–1433. https://doi.org/10.1016/j.rse.2011.01.022.
Senf, C., Pflugmacher, D., Wulder, M.A., Hostert, P., 2015. Characterizing spectral-temporal patterns of defoliator and bark beetle disturbances using Landsat time series. Remote Sens. Environ. 170, 166–177. https://doi.org/10.1016/j.rse.2015.09.019.
SLU, 2019. Skogsdata 2019. Umeå, Sweden.
Sommerfeld, A., Senf, C., Buma, B., D'Amato, A.W., Després, T., Díaz-Hormazábal, I., Fraver, S., Frelich, L.E., Gutiérrez, Á.G., Hart, S.J., Harvey, B.J., He, H.S., Hlásny, T., Holz, A., Kitzberger, T., Kulakowski, D., Lindenmayer, D., Mori, A.S., Müller, J., Paritsis, J., Perry, G.L.W., Stephens, S.L., Svoboda, M., Turner, M.G., Veblen, T.T., Seidl, R., 2018. Patterns and drivers of recent disturbances across the temperate forest biome. Nat. Commun. 9 https://doi.org/10.1038/s41467-018-06788-9.
Sproull, G.J., Adamus, M., Bukowski, M., Krzyzanowski, T., Szewczyk, J., Statwick, J., Szwagrzyk, J., 2015. Tree and stand-level patterns and predictors of Norway spruce mortality caused by bark beetle infestation in the Tatra Mountains. For. Ecol. Manage. 354, 261–271. https://doi.org/10.1016/j.foreco.2015.06.006.
Tanase, M.A., Aponte, C., Mermoz, S., Bouvet, A., Le Toan, T., Heurich, M., 2018. Detection of windthrows and insect outbreaks by L-band SAR: A case study in the Bavarian Forest National Park. Remote Sens. Environ. 209, 700–711. https://doi.org/10.1016/j.rse.2018.03.009.
Trubin, A., Kozhoridze, G., Zabihi, K., Modlinger, R., Singh, V.V., Surový, P., Jakuš, R., 2023. Detection of susceptible Norway spruce to bark beetle attack using PlanetScope multispectral imagery. Front. for. Glob. Chang. 6, 1–15. https://doi.org/10.3389/ffgc.2023.1130721.
Trubin, A., Kozhoridze, G., Zabihi, K., Modlinger, R., Vikram, V., Surový, P., Jakus, R., 2024. Detection of green attack and bark beetle susceptibility in Norway Spruce: Utilizing PlanetScope Multispectral Imagery for Tri-Stage spectral separability analysis. For. Ecol. Manage. 560, 12. https://doi.org/10.1016/j.foreco.2024.121838.
Valbuena, R., Mauro, F., Rodriguez-Solano, R., Manzanera, J.A., 2010. Accuracy and precision of GPS receivers under forest canopies in a mountainous environment. Spanish J. Agric. Res. 8, 1047–1057. https://doi.org/10.5424/sjar/2010084-1242.
Wermelinger, B., 2004. Ecology and management of the spruce bark beetle Ips typographus—a review of recent research. For. Ecol. Manage. 202, 67–82. https://doi.org/10.1016/J.FORECO.2004.07.018.
Wulff, S., Roberge, C., 2023. Inventering av granbarkborreangrepp i Götaland och Svealand. Umeå, Sweden.
Yu, R., Huo, L., Huang, H., Yuan, Y., Gao, B., Liu, Y., Yu, L., Li, H., Yang, L., Ren, L., Luo, Y., 2022. Early detection of pine wilt disease tree candidates using time-series of spectral signatures. Front. Plant Sci. 13, 1–16. https://doi.org/10.3389/fpls.2022.1000093.